Electric Power Components and Systems, 40:1842–1869, 2012

ISSN: 1532-5008 print/1532-5016 online
DOI: 10.1080/15325008.2012.722581

Taylor & Francis
Taylor & Francis Group

A Feedback Linearization Scheme for the Control of Synchronous Generators

ANDREA BONFIGLIO,[1] FEDERICO DELFINO,[1] MARCO INVERNIZZI,[1] ADRIANO PERFUMO,[2] and RENATO PROCOPIO[1]

[1]Department of Naval and Electrical Engineering, University of Genoa, Genova, Italy
[2]Toshiba T&D Europe, Genova, Italy

Abstract *This article proposes an advanced non-linear control algorithm to manage active power and voltage provided by a synchronous generator. The algorithm is based on the so-called feedback linearization theory, which relies on the central concept to algebraically transform non-linear systems dynamics into fully or partly linear ones, so that linear control techniques can be applied. Starting from the basic (electrical, magnetic, and mechanical) machine equations, a suitable state transformation is introduced in order to apply the feedback linearization block to the generator model. A regulation scheme is then derived, which receives as inputs the measure and reference signals of both the electric power and the voltage at the generator side and produces as outputs the physical inputs of the machine,* i.e.*, the mechanical torque and the field voltage. Particular attention is devoted to both the linearization process, where internal dynamics and stability studies play an important role, and to the design of the two (power and voltage) decoupled regulators. Several simulations are finally performed in order to verify the effectiveness of the proposed approach and to highlight its main advantages and drawbacks with respect to the traditional P-V synchronous generator control strategy.*

Keywords synchronous generators, feedback linearization, voltage and power control

1. Introduction

The present way of controlling and regulating generation units is typically based on a linearized model of the system. The strength of this approach is in its simplicity, robustness, and wide application area. However, the synchronous generator is, for its nature, a non-linear dynamic system whose [1–5] main problems involve the dynamic coupling effect between the controlled quantities, namely the electric power delivered and the machine voltage and the presence of electromechanical oscillations. In scientific literature, there is a large variety of methods and procedures to reduce the impact of these problems; for example, the employment of the so-called stabilizing signals allows the mitigation of the electromechanical oscillations phenomena [6].

Received 16 February 2012; accepted 1 August 2012.
Address correspondence to Ing. Andrea Bonfiglio, Department of Naval & Electrical Engineering, University of Genoa, Via Opera Pia 11a, Genova, I-16145, Italy. E-mail: a.bonfiglio@unige.it

Many different control techniques have been studied to find a solution to the problems of the traditional regulation; among these, it is worth citing neural networks (NNs), variable structure control, digital control, self-tuning regulators, and exact linearization methods [7–12]. In light of this state of the art, Ansaldo, Italian leading thermoelectric power plants producer, was moved to start a research program in cooperation with the Power Systems Research Unit at the University of Genoa aimed at developing a prototypal regulator for the synchronous machine based on the so-called feedback linearization (FBL) control theory, which belongs to the family of the exact linearization techniques. More specifically, FBL has been initially adopted for robotic arms, depth positioning of underwater vehicles, active vehicle suspensions, and hydraulic servo systems [13–18]. Lately, this kind of approach has been also used in the electromechanical field, with specific reference to DC motors, active magnetic bearings, filters, and three-phase AC/DC pulse-width modulation (PWM) converters [19–22].

The interest in FBL application resides in the opportunity of creating a linear and decoupled relationship between new fictitious inputs of the system to be controlled and its real outputs. This way, it is possible to apply the classical control technique for linear systems avoiding the linearization problem, usually based on a local linearization, depending on the working point, and needing the use of stabilizing signals to dump the electromechanical oscillations. As far as the employment of FBL-based control schemes for the regulation of synchronous machines is concerned, two works can be mentioned in the scientific literature: the one by Savaresi [23] and the one by Fregene and Kennedy [24]. In [23], the peculiarities of FBL theory applied to a fifth-order model of the synchronous generator are thoroughly discussed, highlighting the capability of such a theory to guarantee high performances over the entire working range, unlike traditional proportional-integral-derivative (PID) based controllers. In [24], FBL was applied in combination with a multi-input–multi-output (MIMO) system representation by means of multi-layer NNs; the use of NNs allows keeping track of the operating conditions of the system and responding appropriately to parameters changing.

The present work follows the research line drawn by [23, 24] and presents three main improvements. The problem of the exact linearization of the third-order model of the synchronous generator, still open according to [23], is solved by means of the addition of an equivalent asynchronous torque, which also enables the effect of the dumpers to be taken into account [25]. This allows adoption of a lower-order model than in [23] (*i.e.*, the fifth one), which limits the computational efforts and error propagation due to both an imperfect knowledge of the model parameters and a higher number of derivatives to linearize the fifth-order model. Second, particular attention is devoted to the system performances in the presence of faults, such as short circuit and transmission lines out of service, highlighting that the proposed control scheme is also effective in those situations. Finally, a complete sensitivity analysis is carried out introducing the sliding-mode (SM) control technique to face the problem of model and parameter uncertainties and measurement errors.

The model derived accepts the mechanical torque and the field voltage as input variables for the synchronous machine, and system outputs are the machine voltage squared and the electromagnetic power. The speed control is not taken into account, since the considered configuration is that of a machine connected via a step-up transformer to an infinite power bus, so the steady state frequency value is fixed to the one of the main grid. The problem of the system internal dynamics that comes from the linearization process is discussed, and the design of two scalar regulators is presented in order to control the system outputs as desired. Finally, starting from the model previously developed, a

traditional control algorithm is applied to the synchronous generator with the aim to verify, by means of several comparative simulations, effectiveness, efficiency, and performances of the new approach. The performed simulations highlighted satisfactory performances of the new control strategy in both steady-state and fault conditions.

2. Problem Formulation

The FBL procedure requires the mathematical system describing the synchronous generator to be written in the following normal form:

$$\begin{cases} \dot{\boldsymbol{x}} = \boldsymbol{f}(\boldsymbol{x}) + \boldsymbol{g}(\boldsymbol{x})\boldsymbol{u}, \\ \boldsymbol{y} = \boldsymbol{h}(\boldsymbol{x}), \end{cases} , \tag{1}$$

where $\boldsymbol{u}$ and $\boldsymbol{y}$ are, respectively, the input and the output vectors; $\boldsymbol{x}$ is the state vector. In order to obtain this representation, the following assumptions have been made:

- the stator resistances are neglected;
- the stator fluxes time derivatives are neglected;
- dampers are not present; and
- in the stator electric equations, the angular frequency is assumed to be constant and equal to the network frequency ω_e.

Under these hypotheses, it is possible to obtain the following expression of the $\boldsymbol{f}$, $\boldsymbol{g}$, and $\boldsymbol{h}$ matrixes, as detailed in Appendix A:

$$\boldsymbol{f}(\boldsymbol{x}) = \begin{bmatrix} \omega_n(\omega - \omega_e) \\ AB\sin 2\delta - AC\Phi_f \sin\delta + \dfrac{K_d}{2H}(\omega_e - \omega) \\ D\Phi_f + E\cos\delta \end{bmatrix}, \tag{2}$$

$$\boldsymbol{g}(\boldsymbol{x}) = \begin{bmatrix} 0 & 0 \\ 0 & -\dfrac{1}{2H} \\ \omega_n & 0 \end{bmatrix}, \tag{3}$$

$$\boldsymbol{h}(\boldsymbol{x}) = \begin{bmatrix} E_h \sin 2\delta + F_h \Phi_f \sin\delta + K_d \omega_e(\omega_e - \omega) \\ A_h \sin^2\delta + B_h \cos^2\delta + C_h \Phi_f^2 + D_h \Phi_f \cos\delta \end{bmatrix}. \tag{4}$$

where A, B, C, D, E, A_h, B_h, C_h, D_h, E_h, and F_h are constant, defined in Appendix A, related to the electric parameters of the system.

3. Problem Solution

Recalling equation (A18), the two outputs y_1 and y_2 can be written as

$$y_1 = h_1(\boldsymbol{x}) = E_h \sin 2x_1 + F_h \sin x_1 + K_d \omega_e(\omega_e - x_2), \tag{5}$$

$$y_2 = h_2(\boldsymbol{x}) = A_h \sin^2 x_1 + B_h \cos^2 x_1 + C_h x_3^2 + D_h x_3 \cos x_1. \tag{6}$$

Now, according to FBL theory [26], it is necessary to derive y_1 and y_2 until one of the two inputs is found. Beginning with the first input,

$$\dot{y}_1 = \nabla \boldsymbol{h_1} \cdot \dot{\boldsymbol{x}} = \nabla \boldsymbol{h_1} \cdot \boldsymbol{f}(\boldsymbol{x}) + \nabla \boldsymbol{h_1} \cdot \boldsymbol{g}(\boldsymbol{x}) \cdot \boldsymbol{u} = L_f h_1 + \boldsymbol{L_g h_1} \cdot \boldsymbol{u}, \tag{7}$$

where the h_1 gradient is equal to

$$\nabla \boldsymbol{h_1} = \begin{bmatrix} \dfrac{\partial h_1}{\partial x_1} & \dfrac{\partial h_1}{\partial x_2} & \dfrac{\partial h_1}{\partial x_3} \end{bmatrix}, \tag{8}$$

and

$$\frac{\partial h_1}{\partial x_1} = 2E_h \cos 2x_1 + F_h x_3 \cos x_1, \tag{9}$$

$$\frac{\partial h_1}{\partial x_2} = -K_d \omega_e, \tag{10}$$

$$\frac{\partial h_1}{\partial x_3} = F_h \sin x_1. \tag{11}$$

Using Eqs. (9), (10), and (11), it is possible to calculate the $L_f h_1$ and $\boldsymbol{L_g h_1} \cdot \boldsymbol{u}$ Lie derivatives [26] as follows:

$$\begin{aligned} L_f h_1 = \nabla \boldsymbol{h_1} \cdot \boldsymbol{f}(\boldsymbol{x}) = {} & 2\omega_n E_h (x_2 - \omega_e) \cos 2x_1 + \omega_n F_h (x_2 - \omega_e) x_3 \cos x_1 + \\ & - K_d \omega_e \left[AB \sin x_1 - AC x_3 \sin x_1 + \frac{K_d}{2H} (\omega_e - x_2) \right] \\ & + DF_h x_3 \sin x_1 + EF_h \cos x_1 \sin x_1 \end{aligned} \tag{12}$$

and

$$\boldsymbol{L_g h_1} \cdot \boldsymbol{u} = \nabla \boldsymbol{h_1} \cdot \boldsymbol{g}(\boldsymbol{x}) \cdot \boldsymbol{u} = F_h \omega_n \sin x_1 u_1 + \frac{K_d \omega_e}{2H} u_2. \tag{13}$$

Both inputs u_1 and u_2 appear in Eq. (13), so the relative degree [26] r_1 of the first output is

$$r_1 = 1. \tag{14}$$

Similarly, repeating the same procedure for the second output gives

$$\dot{y}_2 = \nabla \boldsymbol{h_2} \cdot \dot{x} = \nabla \boldsymbol{h_2} \cdot \boldsymbol{f}(\boldsymbol{x}) + \nabla \boldsymbol{h_2} \cdot \boldsymbol{g}(\boldsymbol{x}) \cdot \boldsymbol{u} = L_f h_2 + \boldsymbol{L_g h_2} \cdot \boldsymbol{u}, \tag{15}$$

where the h_2 gradient is equal to

$$\nabla \boldsymbol{h_2} = \begin{bmatrix} \dfrac{\partial h_2}{\partial x_1} & \dfrac{\partial h_2}{\partial x_2} & \dfrac{\partial h_2}{\partial x_3} \end{bmatrix} \tag{16}$$

and

$$\frac{\partial h_2}{\partial x_1} = (A_h - B_h)\sin 2x_1 - D_h x_3 \sin x_1, \tag{17}$$

$$\frac{\partial h_2}{\partial x_2} = 0, \tag{18}$$

$$\frac{\partial h_2}{\partial x_3} = 2C_h x_3 + D_h \cos x_1. \tag{19}$$

$L_f h_2$ and $\boldsymbol{L_g h_2} \cdot \boldsymbol{u}$ can now be evaluated as

$$L_f h_2 = \nabla \boldsymbol{h_2} \cdot \boldsymbol{f}(\boldsymbol{x}) = \omega_n (A_h - B_h)(x_2 - \omega_e)\sin 2x_1 - \omega_n D_h x_3 (x_2 - \omega_e)\sin x_1$$
$$+ 2C_h D x_3^2 + D D_h x_3 \cos x_1 + 2E C_h x_3 \cos x_1 + E D_h \cos^2 x_1 \tag{20}$$

and

$$\boldsymbol{L_g h_2} \cdot \boldsymbol{u} = \nabla \boldsymbol{h_2} \cdot \boldsymbol{g}(\boldsymbol{x}) \cdot \boldsymbol{u} = (2\omega_n C_h x_3 + D_h \omega_n \cos x_1) u_1. \tag{21}$$

As before, the procedure must be stopped at the first-order derivative, since the first input appears, fixing therefore the value of the second output relative degree to 1:

$$r_2 = 1. \tag{22}$$

It is now possible to determine the total relative degree of the system, as the sum of the two relative degrees [26]:

$$r = r_1 + r_2 = 2. \tag{23}$$

Since the dynamic order of the system is 3 and the total relative degree r is 2, the state transformation must be completed with another component whose dynamics is unobservable and must be analyzed in order to verify the stability properties of the whole system. This issue will be thoroughly discussed in the next section.

Indicating the regulator outputs with v_1 and v_2 and imposing them equal to the first derivatives of the machine outputs, the system to be controlled is equal to two simple and decoupled integrators, as depicted in Figure 1.

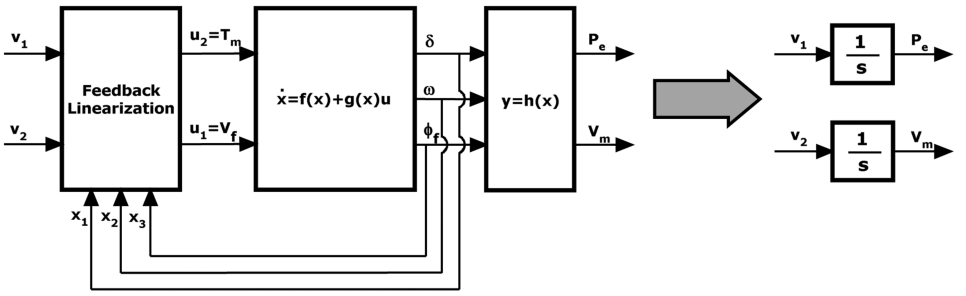

Figure 1. FBL equivalent block diagram.

However, since the real system inputs are u_1 and u_2, it is necessary to establish a relationship between the couples v_1 and v_2 and u_1 and u_2. Therefore, recalling Eqs. (12), (13), (20), and (21),

$$v_1 = \dot{P}_e = L_f h_1(\boldsymbol{x}) + (\omega_n F_h \sin\delta)u_1 + \frac{K_d \omega_e}{2H}u_2, \tag{24}$$

$$v_2 = \dot{V}_m^2 = L_f h_2(\boldsymbol{x}) + \omega_n(2C_h\Phi_f + D_h\cos\delta)u_1. \tag{25}$$

By inverting these two equations, it is possible to determine the above-mentioned relations as

$$u_1 = V_f = \frac{v_2 - L_f h_2(\boldsymbol{x})}{\omega_n(2C_h\Phi_f + D_h\cos\delta)} \tag{26}$$

and

$$u_2 = T_m = \frac{v_1 - L_f h_1(\boldsymbol{x}) - F_h\sin\delta\left(\dfrac{v_2 - L_f h_2(\boldsymbol{x})}{2C_h\Phi_f + D_h\cos\delta}\right)}{\dfrac{K_d\omega_e}{2H}}. \tag{27}$$

Such relations are implemented in the FBL block.

It is worth noting that the system is always invertible except for the case when

$$(2C_h\Phi_f + D_h\cos\delta) = 0, \tag{28}$$

$$K_d = 0. \tag{29}$$

Equation (29) highlights the necessity of an equivalent damping factor in order to perform a complete linearization of the system [23].

Furthermore, manipulating Eq. (28), the condition to be avoided can be rewritten in order to succeed in designing the FBL block, *i.e.*,

$$V_{mq} = 0. \tag{30}$$

4. Internal and Zero Dynamics

As previously discussed, the system has a new state that consists of P_e and V_m^2. The third component is the one that characterizes the so called *internal dynamics*. It has to be a scalar function of the states $\Psi(x_1, x_2, x_3)$ that satisfy the following relation [26]:

$$\nabla\boldsymbol{\Psi}\cdot(\boldsymbol{g}(\boldsymbol{x})\cdot\boldsymbol{u}) = 0. \tag{31}$$

Solving the scalar product gives

$$\nabla\boldsymbol{\Psi}\cdot(\boldsymbol{g}(\boldsymbol{x})\cdot\boldsymbol{u}) = -\frac{\partial\Psi}{\partial x_2}\frac{u_2}{2H} + \frac{\partial\Psi}{\partial x_3}\omega_n u_1 = 0. \tag{32}$$

The previous equation must be satisfied for any input u_1 and u_2, so it must be

$$\begin{cases} \dfrac{\partial\Psi}{\partial x_2} = 0, \\ \dfrac{\partial\Psi}{\partial x_3} = 0. \end{cases} \tag{33}$$

It can be concluded that $\Psi(\cdot)$ must be a function only of the first component x_1:

$$\Psi = \Psi(x_1). \tag{34}$$

The simplest function possible is chosen as:

$$\Psi(x_1) = x_1. \tag{35}$$

Now the state of the transformed system is univocally defined:

$$\boldsymbol{z} = \begin{bmatrix} P_e & V_m^2 & \delta \end{bmatrix}. \tag{36}$$

Nevertheless, the condition in Eq. (33) is necessary but not sufficient to guarantee that the state transformation

$$z = f(x) \tag{37}$$

is one-to-one.

The Jacobean matrix of the transformation is calculated and its determinant evaluated. After simple mathematical operations, one obtains that

$$\det \begin{bmatrix} \dfrac{\partial P_e}{\partial \delta} & \dfrac{\partial P_e}{\partial \omega} & \dfrac{\partial P_e}{\partial \Phi_f} \\ \dfrac{\partial V_m^2}{\partial \delta} & \dfrac{\partial V_m^2}{\partial \omega} & \dfrac{\partial V_m^2}{\partial \Phi_f} \\ \dfrac{\partial \delta}{\partial \delta} & \dfrac{\partial \delta}{\partial \omega} & \dfrac{\partial \delta}{\partial \Phi_f} \end{bmatrix} = -K_d \omega_e (2C_h \Phi_f + D_h \cos\delta). \tag{38}$$

It can be noticed that the conditions for which the determinant is non-zero are the same that were necessary to create the linearization block.

In conclusion, the following invertible state transformation exists:

$$\begin{bmatrix} P_e \\ V_m^2 \\ \delta \end{bmatrix} = \boldsymbol{\varphi}(\delta \quad \omega \quad \Phi_f) = \begin{bmatrix} E_h \sin 2\delta + F_h \Phi_f \sin\delta + K_d \omega_e(\omega_e - \omega) \\ A_h \sin^2\delta + B_h \cos^2\delta + C_h \Phi_f^2 + D_h \Phi_f \cos\delta \\ \delta \end{bmatrix}. \tag{39}$$

Equations (24) and (25) show that the dynamics of the external part does not present any stability problem; the same cannot be said for the unobservable internal dynamics, for which the stability condition is not assured and could lead the whole system to instability.

The stability properties of the internal dynamics can be deduced by studying the stability of the so called "zero dynamics" configuration. This dynamics is obtained by setting the observable part of the new state to its equilibrium value [26]:

$$\begin{cases} P_e = P_{e0}, \\ V_m^2 = V_{m0}^2, \\ \dot{\delta} = f\left(V_{m0}^2, P_{eo}, \delta\right) = \omega_n \left[\omega\left(V_{m0}^2, P_{eo}, \delta\right) - \omega_e\right]. \end{cases} \tag{40}$$

The machine speed must be expressed as a function of the new state components, solving the system

$$\begin{cases} P_e = E_h \sin 2\delta + F_h \Phi_f \sin\delta + K_d \omega_e(\omega_e - \omega), \\ V_m^2 = A_h \sin^2\delta + B_h \cos^2\delta + C_h \Phi_f^2 + D_h \cos\delta \Phi_f, \quad . \\ \delta = \delta \end{cases} \tag{41}$$

After some algebraic manipulation of Eqs. (40) and (41), and considering Eqs. (A6)–(A13) and (A26), one can easily reach the following expression for the zero dynamic of the system:

$$\dot{\delta} = \frac{\omega_n}{K_d \omega_e} \left(P_{e0} - \left(E_h - \frac{F_h D_h}{4C_h} \right) \sin 2\delta - \frac{F_h}{\sqrt{C_h}} \sqrt{V_{m0}^2 - A_h \sin^2\delta} \sin\delta \right). \tag{42}$$

The internal dynamics is asymptotically stable if the zero dynamic is locally asymptotically stable [26]. The stability of the zero dynamics has been verified for a set of points from 3 to −3 radians.

5. Regulators Design

Due to the position in Eq. (25), it is possible to design the regulators as follows: the electromagnetic power controller is driven by the difference between the reference value P_{eref} (the references are supposed to be constant since typically only step variations are required) and the measured value of the electromagnetic power P_e. The function implemented in it can simply be a positive gain, thus obtaining

$$v_1 = K_P (P_{eref} - P_e). \tag{43}$$

Equations (43) and (24) lead to the following differential equation for P_e:

$$\dot{P}_e + K_P P_e = K_P P_{eref}, \tag{44}$$

whose unique solution is

$$P_e(t) = P_{eref} + (P_{e0} - P_{eref}) e^{-K_P t}. \tag{45}$$

The same applies to the voltage channel, resulting in the following regulation law:

$$v_2 = K_V \left(V_{mref}^2 - V_m^2 \right), \tag{46}$$

with K_V being a positive gain and V_{mref}^2 the desired value for the squared machine voltage. This leads to the solution

$$V_m^2(t) = V_{mref}^2 + \left(V_{m0}^2 - V_{mref}^2 \right) e^{-K_V t}. \tag{47}$$

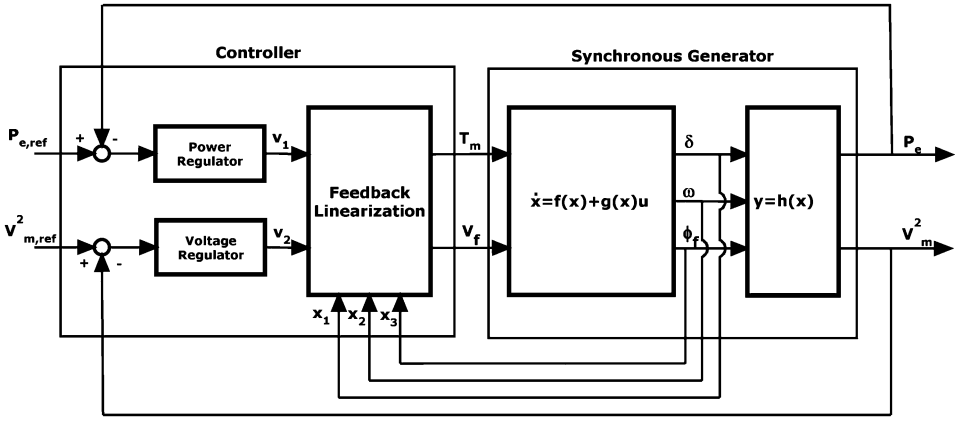

Figure 2. Scheme of the whole control system.

By focusing attention on Eqs. (44) and (47), it is noticed that by regulating the gains K_P and K_V, the response profile of the two outputs can be decided. In order to match the typical dynamics response of the controlled output, the two gains have been set as

$$\begin{cases} K_P = 1 \\ K_V = 5 \end{cases}. \tag{48}$$

In Figure 2, the block-scheme of the whole system configuration is plotted.

The design of the two regulation channels could have followed a different strategy implementing different structures of the regulators, such as proportional-integral (PI) or lead-lag type. Nevertheless, the simulation conducted to test the other types of regulators, avoided here for the sake of brevity, highlighted that the proportional regulation guarantees the best performance of the controlled output time response in terms of rise time and oscillations of the controlled outputs.

6. Traditional Regulation

As far as the traditional regulation of the synchronous generator is concerned, the scheme of the primary and secondary regulation is taken into account here [2].

It consists of two loops, an active power control loop and a machine voltage one. The power control loop is superimposed onto the frequency control one, and its regulator is typically a conventional PI controller.

Its transfer function is of the kind

$$g_p(s) = k_p \frac{1 + sT_p}{sT_p}, \tag{49}$$

where T_p is a time constant, and k_p is the power loop gain, whose values are

$$\begin{cases} k_p = 0,4 \text{ p.u.} \\ T_p = 13 \text{ sec} \end{cases}. \tag{50}$$

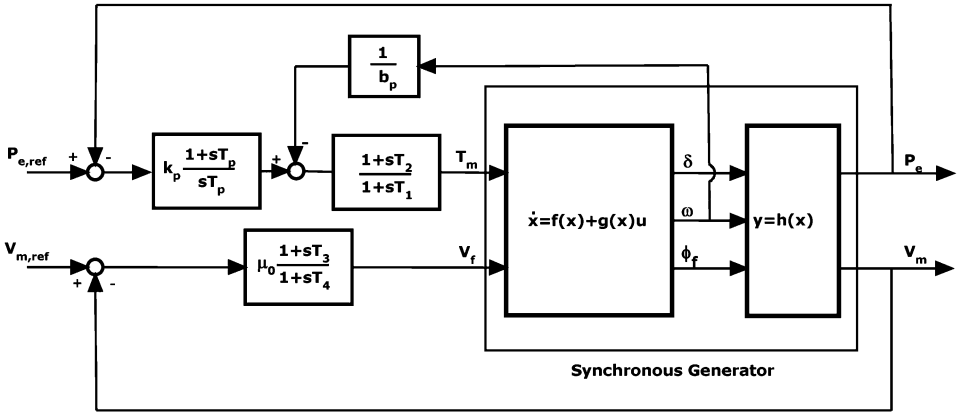

Figure 3. Block diagram of the traditional control system.

The purpose of this scheme is to obtain the reference angle for the frequency loop. In such a control loop, b_p is the droop, whose value is $b_p = 0,05$, and the actuators transfer function is a lead-lag:

$$g_{ac}(s) = \frac{1 + sT_2}{1 + sT_1}, \tag{51}$$

where T_1 and T_2 are time constant whose values are

$$\begin{cases} T_1 = 15 \text{ sec} \\ T_2 = 5 \text{ sec} \end{cases}. \tag{52}$$

The machine voltage control loop is obtained considering a system static excitation constant μ_0 and two time constants T_3 and T_4, whose values now are

$$\begin{cases} \mu_0 = 400 \\ T_1 = 20 \text{ sec} \\ T_2 = 1 \text{ sec} \end{cases}. \tag{53}$$

The block diagram of the traditional control strategy detailed above is depicted in Figure 3 [6].

7. Simulations and Results

In order to test the efficiency of FBL regulation, a comparative analysis with the traditional control method has been performed. Four types of events have been considered, namely:

- variation of the power reference,
- variation of the voltage reference,
- variation of the connection reactance, and
- shot circuit at the point of common coupling (PCC).

The disturbances are applied to the system separately and starting from an equilibrium condition. For each case, the examined quantities are the system inputs, state, and outputs, described in Section 2. In all pictures, the results obtained by resorting to the FBL approach are reported in continuous lines, while the dotted lines represent the same quantities as given by the traditional regulation. In order to make the simulations closer to the real scenario, one has to impose limits on the outputs of the control system and constraints on the variation of physical quantities. For this reason, a limit was set on the absolute value of the field voltage of 6 p.u., and upper and lower limits on the mechanical torque set to 1 p.u. and 0.3 p.u., respectively. Moreover, since in the real configuration, very fast variations of the mechanical torque are not allowed, a limit was put on the torque gradient. The limit applied is 2 p.u./s when the valves are closing (torque is decreasing) and 0.7 p.u./s when the valves are opening (torque is increasing) [6].

7.1. Variation of the Power Reference

The variation of the power reference has been examined giving the systems—traditional and FBL—a step whose amplitude is

$$\Delta P_e = 0.15 \text{ p.u.} \tag{54}$$

As shown in Figure 4, the FBL control scheme exhibits a better system dynamics response with respect to the classical one and is in line with the expectations on the time response behavior (see Section 5). Figure 5 shows how the FBL approach decouples the power and the voltage control channels, since the machine voltage is constant during the transient.

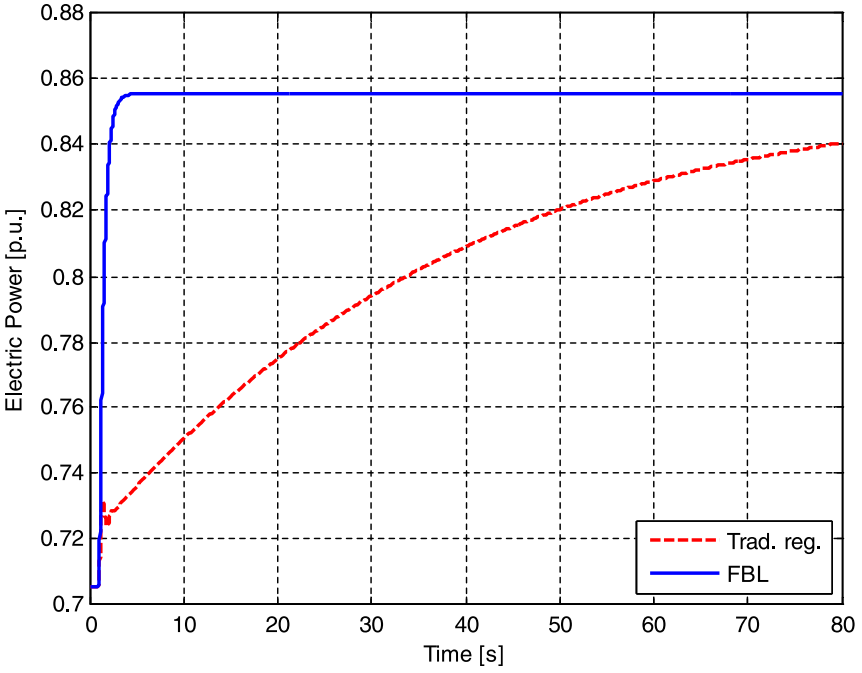

Figure 4. Electric power reference variation: electric power time profile. (color figure available online)

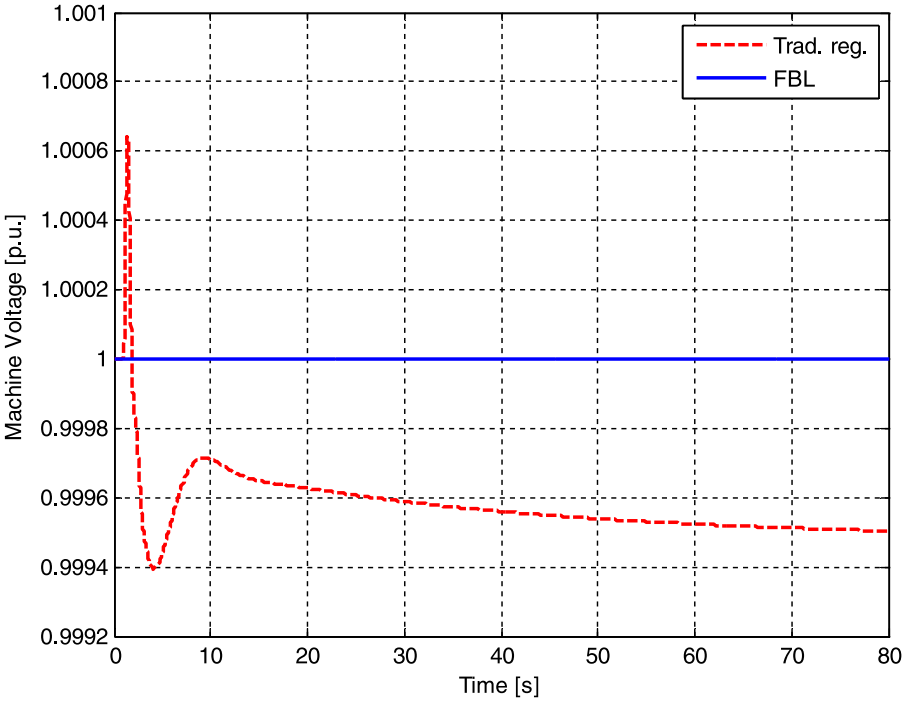

Figure 5. Electric power reference variation: machine voltage time profile. (color figure available online)

7.2. *Variation of the Voltage Reference*

As for the previous case, a step in the voltage reference has been applied to both systems. The amplitude of such a step variation has been fixed as

$$\Delta V_m = 0.05 \text{ p.u.} \tag{55}$$

Again, the FBL control scheme is characterized by positive effects on system dynamics. It is not shown here for the sake of brevity, but it has been verified that the machine speed and field voltage dynamics become less oscillatory. Figure 6 shows how the FBL control decoupling is lost for a brief time due to the fact that the torque reaches the maximum allowed gradient; however, the variation is much smaller than that obtained with the traditional regulation. Figure 7 shows how the FBL control technique avoids overshoots in the voltage profile and allows removal of the steady-state error.

7.3. *Comparison with Artificial-intelligence-based Controllers*

As far as innovative control strategies are concerned, algorithms based on artificial intelligence are worth considering. On this subject, progress has been made by researchers since the first application of NNs in the field of power system control, and this technique can be now considered as consolidated.

Therefore, in the present section, the performances of the FBL control strategy are compared with the NN-based control algorithm proposed in [27] for the regulation of the synchronous generator in an identical configuration as that under investigation here

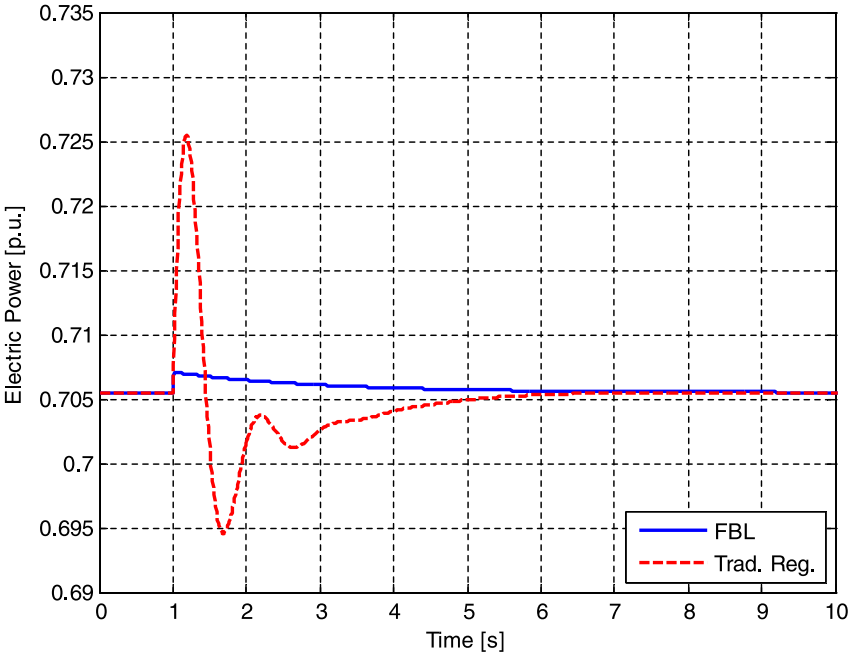

Figure 6. Machine voltage reference variation: electric power time profile. (color figure available online)

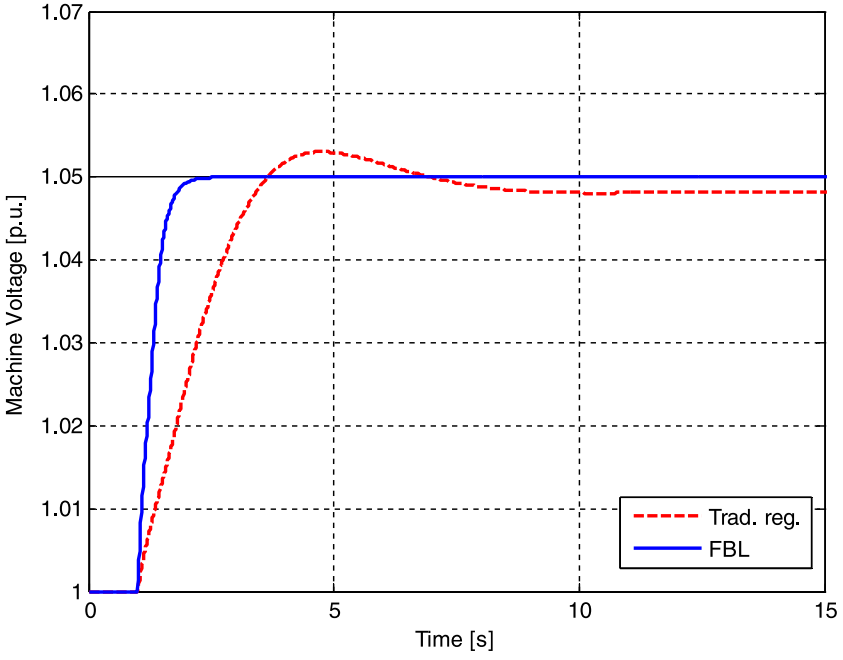

Figure 7. Machine voltage reference variation: machine voltage time profile. (color figure available online)

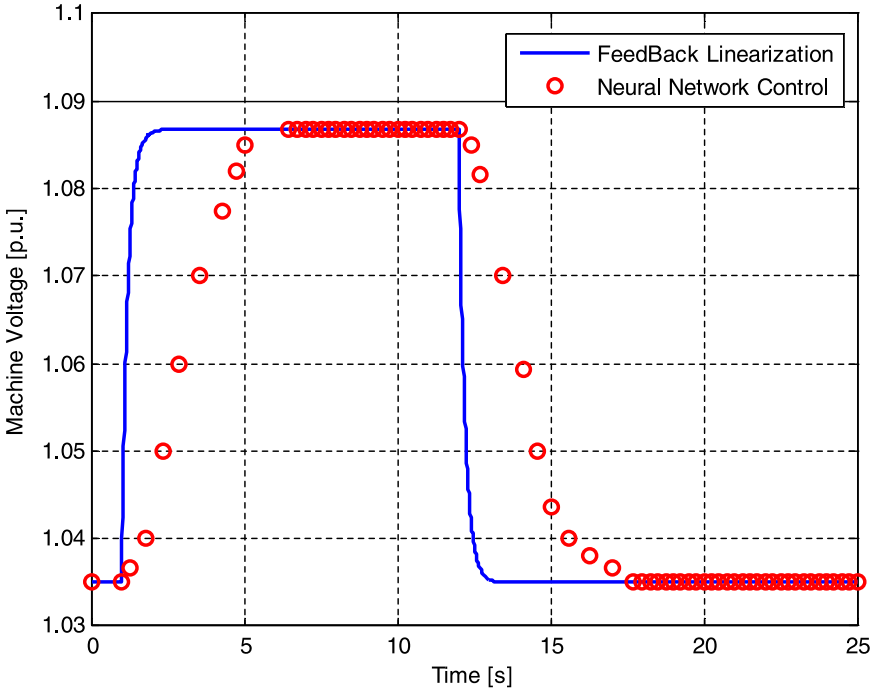

Figure 8. Voltage reference variation: comparison between FBL and NN control. (color figure available online)

(machine connected to an infinite bus). The comparison between the NN and the FBL control strategies is performed considering a 5% step increasing of the terminal voltage reference from the value of 1.035 p.u. at time 1 sec. The voltage reference is then brought back to its original value at 11 sec.

Figure 8 represents the time profile of the machine terminal voltage; as one can notice, both control techniques allow for following the reference variation without steady-state error. Nevertheless, the FBL control strategy presents a faster time response and, thus, a minor time to reach the desired voltage value.

7.4. Variation of the Connection Reactance

The connection reactance variation has been carried out considering the case in which a loss of a connection line occurs at 1 sec, resulting in the following increased value of X:

$$X = 0,24 \text{ p.u.} \tag{56}$$

Under this fault condition, the FBL control strategy gives a better performance for the dynamics of the electric power, machine voltage, and machine frequency. In Figure 9, the absence of steady-state error on the machine voltage in the FBL results can be appreciated. Voltage overshoot is also lower and its dynamics less oscillatory. In addition, the speed has a smaller amplitude perturbation and a non-oscillatory time response, as shown in Figure 10.

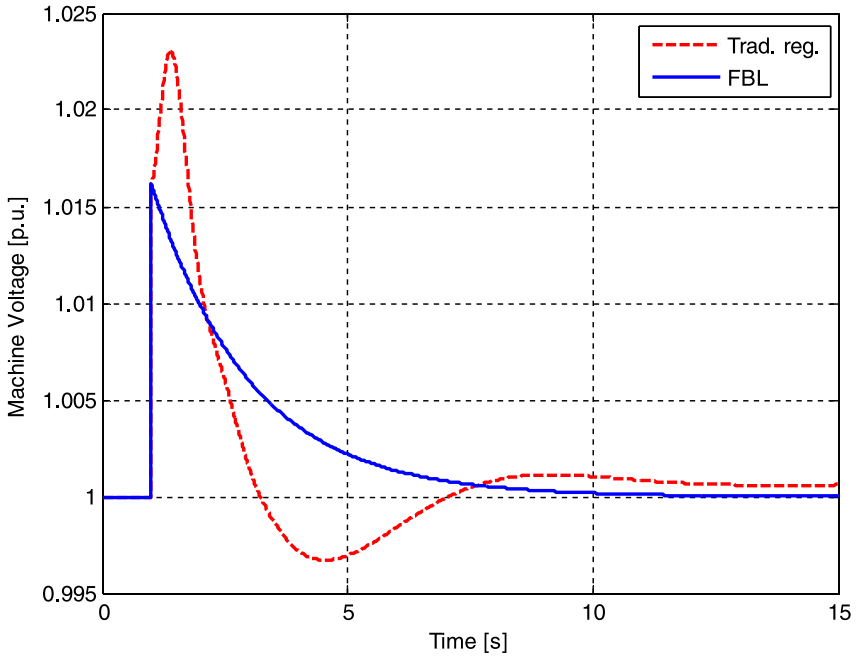

Figure 9. Reactance variation: machine voltage time profile. (color figure available online)

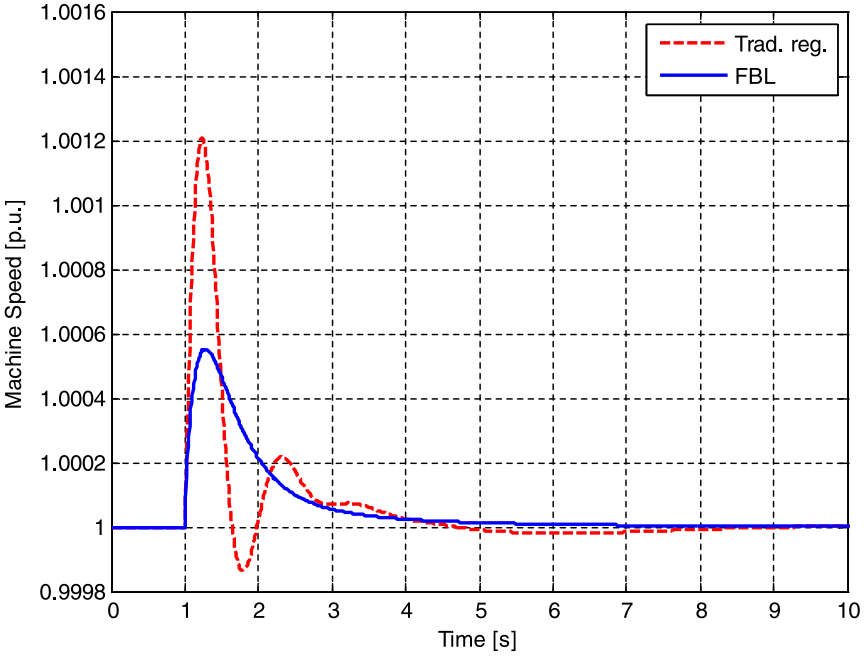

Figure 10. Reactance variation: machine speed time profile. (color figure available online)

7.5. Short Circuit at the PCC

This scenario has been selected to test the performance of the new control strategy under failure condition. The short circuit has been simulated as voltage sag at the PCC. Details on the connection between the fault in a network and voltage sag were given in [28, 29]. The time profile of the network voltage during the short circuit is characterized by a step drop from the steady-state value to zero at a time of 1 sec; the voltage stays at zero from 0.625 sec, and then starts to rise to its previous steady-state value with a ramp that lasts 2 sec. This profile represents the time behavior given by U.S. Federal Energy Regulatory Commission (FERC) and the Canadian Alberta Electric System Operator (AESO) for the LVRT [30]. Figures 11–13 show, respectively, the electric power, machine voltage, and machine speed in such a configuration. In all of those cases, the FBL approach produces faster and less oscillatory responses. The machine speed has a reduction of the maximum and minimum value reached during the transient, which could help in avoiding the trip of speed protections. Furthermore, the machine voltage has basically no dangerous overshoots. Also the short circuit current is reduced, as can be seen in Figure 14.

It is worth highlighting how a short circuit could lead to match condition in Eq. (30) that represents a singularity in the FBL block; nevertheless, the monitoring of the time profile of the machine voltage quadrature component during the short circuit, omitted here for brevity, shows that even if the PCC voltage reaches zero value, the quadrature component is always different from zero. The condition in Eq. (30) could be satisfied only in the case of a three-phase short circuit at the physical connections of the machine. Even if this is a rare condition, this would not destabilize the control strategy, as this

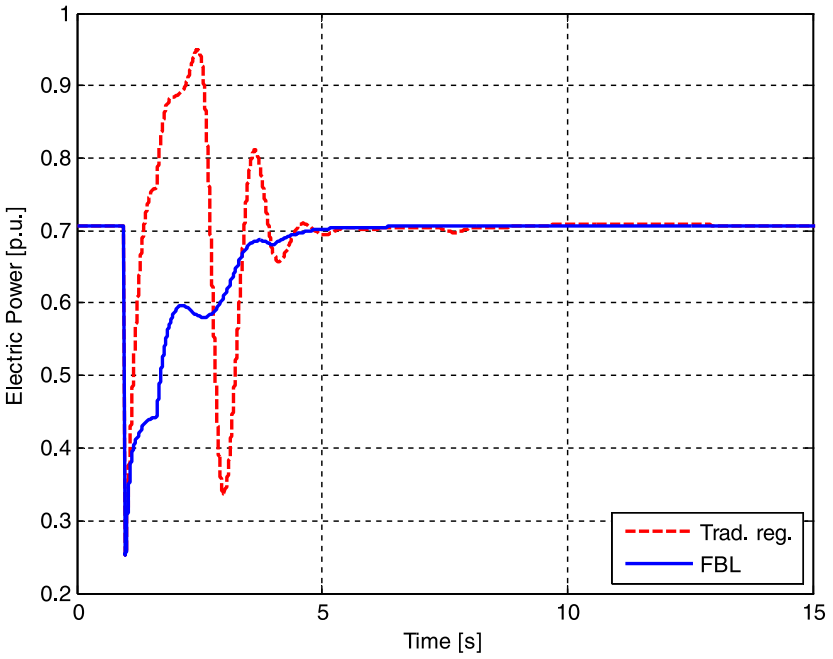

Figure 11. Short circuit: electric power time profile. (color figure available online)

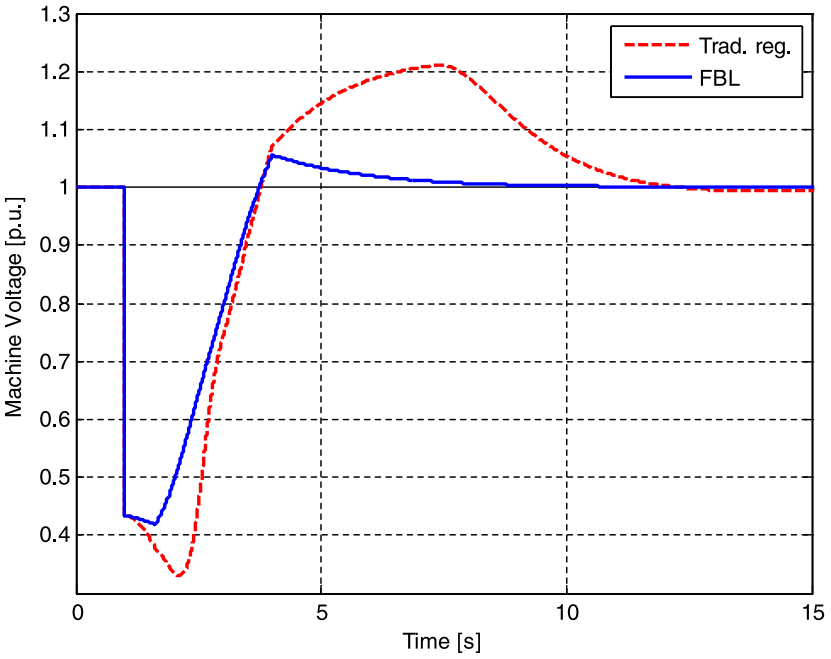

Figure 12. Short circuit: machine voltage time profile. (color figure available online)

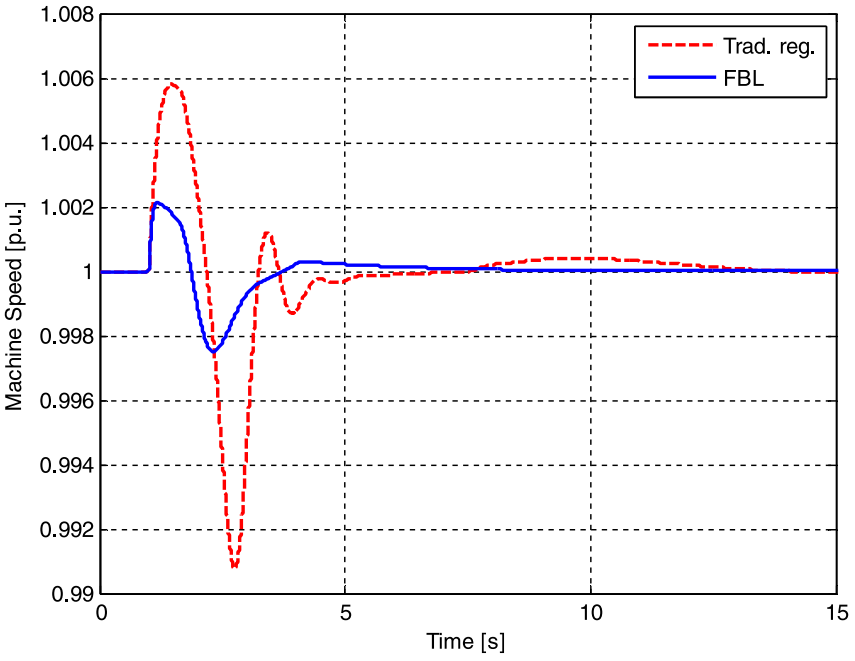

Figure 13. Short circuit: machine speed time profile. (color figure available online)

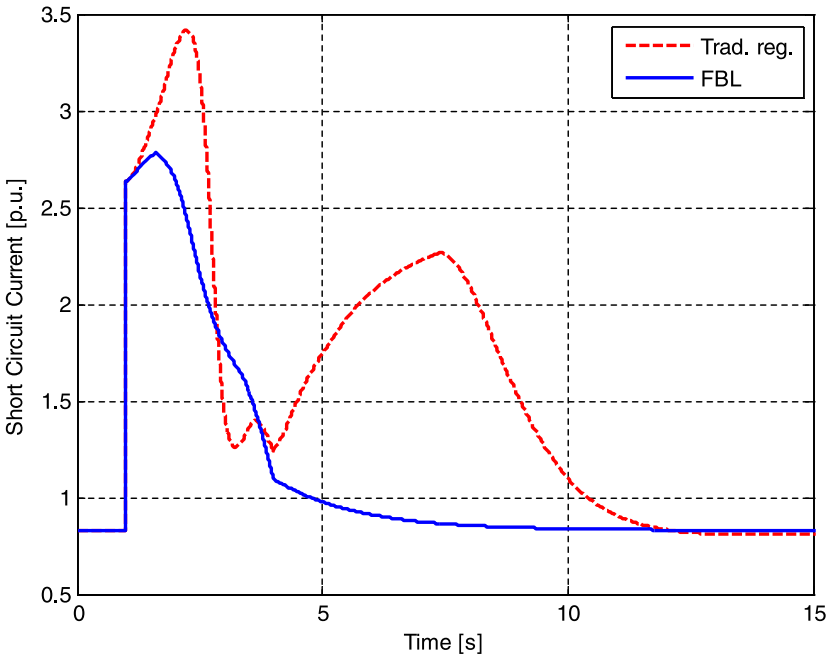

Figure 14. Short-circuit current. (color figure available online)

would result in a saturation of the torque output until *Vmq* returns to values different from zero.

8. Sensitivity Analysis

The FBL technique is unfortunately sensitive to model uncertainties and needs to know the exact values of the state components of the original system. In several cases, the uncertainties drawn from the system model approximations and from the imperfect knowledge of its parameters and variables do not significantly affect the performances of the control system, as this can be circumvented by accurate tuning of the FBL block constants. Nevertheless, in some cases, the approximation error is too wide and cannot be neglected as it could affect the stability and performances of the control algorithm. In these cases, as suggested in [26], the only way to overcome this problem is the integration of the FBL control strategy with the so-called SM control technique.

The SM control technique allows facing with both parametric and model uncertainties. Now consider the application of such a theory to the proposed control scheme in order to overcome the possible destabilizations introduced by model and parameters uncertainties.

In the present configuration, three quantities cannot be measured: the angle δ, the reactance X, and the field flux ϕ_f. Moreover, the SM theory gives the possibility to choose a simpler model for the system to be controlled.

Here, in order to fully exploit the main features of the technique, two single-input–single-output (SISO) systems are used:

- the system consisting of the flux dynamics modeled respectively in Eq. (A21) and Eq. (A22) and of the voltage profile represented in Eq. (A25) for the voltage channel;
- the simplified second-order model for the power channel described by the following equations:

$$\begin{cases} \dot{\delta} = \omega_n(\omega - \omega_e) \\ \dot{\omega} = \dfrac{k}{2H}\sin\delta - \dfrac{T}{2H} \\ P_e = k\sin\delta \end{cases}, \tag{57}$$

  in which k is an unknown constant, depending on the field flux and on the reactance X.

Applying the FBL procedure to the system in Eq. (57), one obtains that the state transformation is

$$\begin{cases} z_1 = P_e = k\sin\delta \\ z_2 = \dot{z}_1 = k\omega_n\cos\delta(\omega - \omega_e) \end{cases}, \tag{58}$$

and its dynamics are

$$\begin{cases} \dot{z}_1 = z_2 \\ \dot{z}_2 = -k\omega_n(\omega - \omega_e)^2\sin\delta - \dfrac{k^2\omega_n}{4H\omega_e}\sin 2\delta + \dfrac{k\omega_n\cos\delta}{2H}T = v \end{cases}, \tag{59}$$

resulting in the following control law:

$$T = \left(v + k\omega_n(\omega - \omega_e)^2\sin\delta + \frac{k^2\omega_n}{4H\omega_e}\sin 2\delta\right)\frac{2H}{k\omega_n\cos\delta}. \tag{60}$$

In order to overcome the problem of the inaccurate knowledge of angle δ, one can observe that

$$\begin{cases} \delta = a\sin\dfrac{z_1}{k} \\ z_2 = \omega_n\sqrt{k^2 - z_1^2}(\omega - \omega_e) \end{cases}. \tag{61}$$

As a consequence, the system dynamics are given by

$$\ddot{z}_1 = f(z) + b(z)T, \tag{62}$$

being

$$f(z) = -z_1\omega_n^2(\omega - \omega_e)^2 - \frac{\omega_n z_1\sqrt{k^2 - z_1^2}}{2H\omega_e} \tag{63}$$

and

$$b(z) = \frac{\sqrt{k^2 - z_1^2}\omega_n}{2H}, \tag{64}$$

where all uncertainties are hidden in the coefficient $k \in [k_{\min}, k_{\max}]$. Indicating the approximations of the functions f and b with f_a, and b_a (obtained by inserting an approximate value k_a for the coefficient k into Eqs. (63) and (64)), one has that the upper bounds F and β on the difference between f and f_a and on the ratio between b and b_a are given by

$$F(z) = \frac{\omega_n z_1}{2H\omega_e}\left(\sqrt{k_{\max}^2 - z_1^2} - \sqrt{k_a^2 - z_1^2}\right) \tag{65}$$

and

$$\beta = \frac{k_{\max}}{\sqrt{k_{\min}^2 - 1}}. \tag{66}$$

So, following the procedure detailed in [26], one has

$$T = \frac{1}{b_a(z)}\left[\hat{u} - K_{sm} \cdot sat\left(\frac{s}{\phi}\right)\right] \tag{67}$$

being

$$\hat{u} = -f_a(z) - \lambda(\dot{z}_1 - \dot{z}_{1ref}) + \dot{z}_{2ref}, \tag{68}$$

$$s = \dot{z}_1 - \dot{z}_{1ref} + \lambda(z_1 - z_{1ref}), \tag{69}$$

and

$$K_{sm} = (F(z) + \eta)\beta + (\beta - 1)|\hat{u}|, \tag{70}$$

in which λ, Φ, and η are three positive constants [26]; *sat* is the saturation function.

As far as the voltage channel is concerned, it is possible to estimate the field flux using Eq. (A25), and recalling that the machine voltage can be measured and that

$$\begin{cases} \sin\delta = P/k_a \\ \cos\delta = 1/k_a\sqrt{k_a^2 - P^2} \end{cases}, \tag{71}$$

the dynamics of the machine voltage can be expressed as

$$\dot{V}_m^2 = (2C_{ha}\phi_f + D_{ha}\cos\delta_a)(\omega_n D_a\phi_f + \omega_n E_a\cos\delta_a) + \omega_n(2C_{ha}\phi_f + D_{ha}\cos\delta_a)v_f, \tag{72}$$

in which subscript a is used to indicate all the quantities that are not known exactly.

With the same meaning of the symbols as before, one has that

$$\begin{cases} f_a = (2C_{ha}\phi_f + D_{ha}\cos\delta_a)(\omega_n D_a\phi_f + \omega_n E_a\cos\delta_a) \\ b_a = \omega_n(2C_{ha}\phi_f + D_{ha}\cos\delta_a) \end{cases} \tag{73}$$

and

$$\begin{cases} |f - f_a| \leq (2C_{ha\,\max}\phi_{f\,\max} + D_{ha\,\max})(\omega_n |D_{a\,\max}|\phi_{f\,\max} + \omega_n E_{a\,\max}) - f_a = F \\ \beta = \dfrac{2C_{ha\,\max}\phi_{f\,\max} + D_{ha\,\max}}{2C_{ha\,\min}\phi_{f\,\min}} \end{cases}. \tag{74}$$

Finally, applying a control law of the same form as Eq. (67), one can obtain the input V_f for the generator, namely

$$V_f = \frac{\left(\hat{u} - k_{sm} \cdot sat\left(\dfrac{s}{\phi_f}\right)\right)}{b_a}, \tag{75}$$

being

$$s = V_m^2 - V_{m,ref}^2, \tag{76}$$

$$k_{sm} = (F + \eta)\beta + (\beta - 1)|\hat{u}|, \tag{77}$$

and

$$\hat{u} = -f_a + \dot{V}_{m,ref}^2. \tag{78}$$

Combining the two channels, the control scheme sketched in Figure 15 can be derived.

In order to evaluate the performance of this control strategy, two step reference variations have been considered, namely a step variation of the electric power reference from 0.85 p.u. to 0.95 p.u. at 1 sec and a step variation to the machine voltage from 1 p.u. to 1.02 p.u. at 5 sec.

Figures 16 and 17 show how the performances of the FBL control in combination with the SM technique are very similar to those provided by the application of only the FBL. The increased robustness of the obtained control strategy is paid with a slight loss of decoupling between the controlled variables.

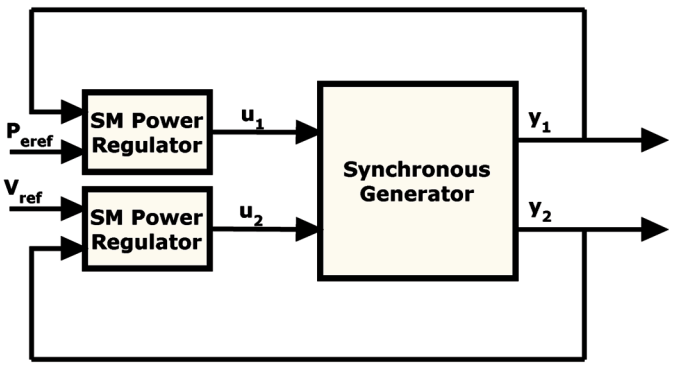

Figure 15. FBL+SM control scheme. (color figure available online)

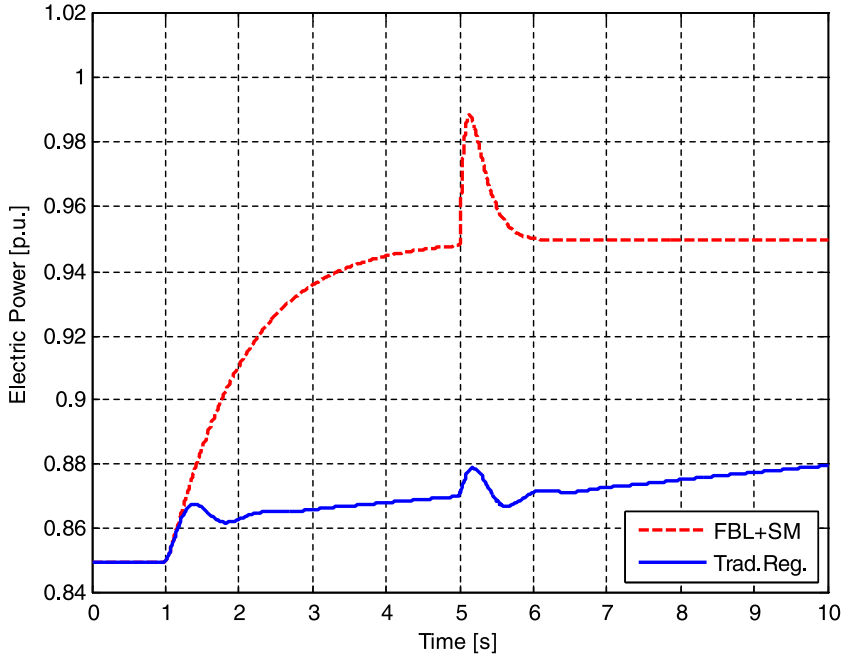

Figure 16. Electric power time profile due to the variation of power and voltage references. (color figure available online)

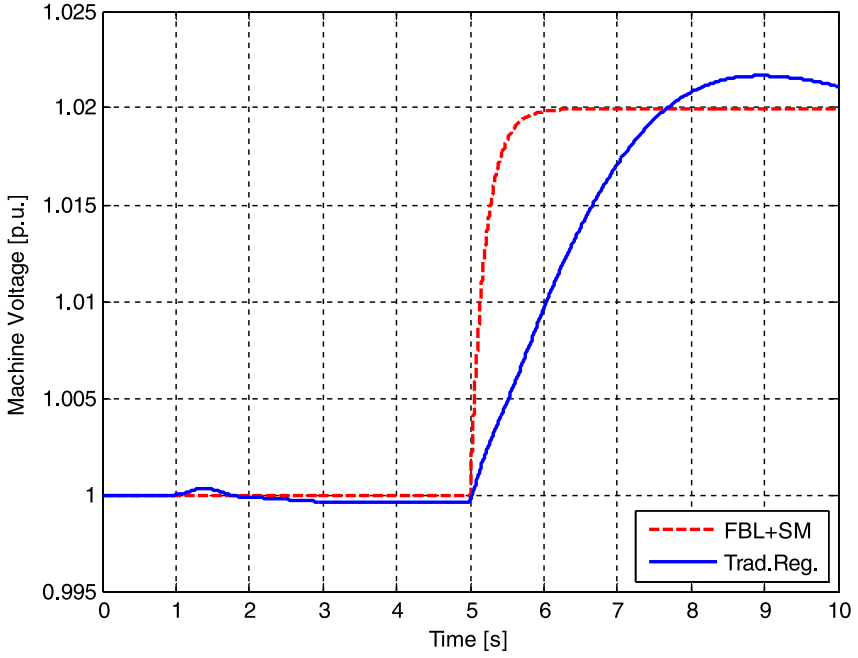

Figure 17. Machine voltage time profile due to the variation of power and voltage references. (color figure available online)

9. Conclusions and Perspectives of Future Work

In this article, a novel FBL-based control scheme to regulate both voltage and active power on a synchronous generator has been proposed. Such a scheme relies on the development of the machine model, on the successive building of a suitable state variable transformation for the system, and on the design of the regulators. Then, a comparison between the results provided by the standard approach and those obtained by resorting to the developed control technique has been proposed in order to verify effectiveness, efficiency, and performance of the latter. The performed simulations show perfect decoupling of the regulation channels and better dynamic response of the machine physical quantities. It is worth noting that the FBL approach also allows the time response dynamics of the controlled quantities to be set simply by modifying the static gain of the regulators, and it is much more robust under failure conditions, such as short circuit and the loss of a connecting line. In the last section, a brief sensitivity analysis has been conducted in order to face the problem of model uncertainties. Work is now in progress together with an industrial partner to apply the FBL control scheme to regulate pressure and temperature of a combustion chamber in a combined cycle power plant.

References

1. Saccomanno, F., *Electric Power System: Analysis and Control*, New York: Wiley–IEEE Press, 2003.
2. Anderson, P. M., and Fouad, A. A., *Power System Control and Stability*, 2nd ed., New York: Wiley–IEEE Press, 2002.
3. Kundur, P., "Control of active and reactive power," in *Power System Stability and Control*, New York: McGraw-Hill, Chap. 11, pp. 581–698, 1994.
4. Ilić, M., and Zaborszky, J., *Dynamics and Control of Large Electric Power Systems*, New Jersey: Wiley (Interscience Division), 2000.
5. Brasca, C. L., and Johnson, M. A., "On automatic voltage regulator design for synchronous generators," *IEEE Trans. Energy Convers.*, Vol. 11, No. 2, pp. 429–434, 1996.
6. Marconato, R., *Electric Power Systems Vol. 2: Steady-State Behaviour, Controls, Short-Circuits and Protection Systems*, Milan: CEI, Chaps. 10 and 11, 2008.
7. Alanis, A. Y., Sanchez, N. E., and Loukianov, A. G., "Discrete-time backstepping neural control for synchronous generators," *Proceedings of the International Joint Conference on Neural Networks (IJCNN 2007)*, pp. 2569–2574, Orlando, FL, 12–17 August 2007.
8. Felix, R. A., Sanchez, E. N., and Loukianov, A. G., "Synchronous generator control combining sliding modes and neural networks," *Proc. Amer. Control Conf.*, Vol. 5, pp. 4065–4070, 4–6 June 2003, Mexico City.
9. Kamalasadan, S., and Swann, G. D., "An intelligent hybrid controller for speed control and stabilization of synchronous generator," *Proceedings of the International Joint Conference on Neural Networks (IJCNN 2009)*, pp. 1481–1488, Atlanta, GA, 14–19 June 2009.
10. Kanniah, J., Malik, O. P., and Hope, G. S., "Excitation control of synchronous generators using adaptive regulators Part I - Theory and simulation results," *IEEE Trans. Power Apparat. Syst.*, Vol. PAS-103, No. 5, pp. 904–910, 1984.
11. Fernandes, M. V. A., Lima, A. D., and Araujo, A. D., "Variable structure model reference adaptive controller applied to a synchronous generator control," *Proceedings of the 16th Mediterranean Conference on Control and Automation*, pp. 635–640, Ajaccio, France, 25–27 June 2008.
12. Erceg, G., Erceg, R., and Erceg, I., "Concepts of synchronous generator's digital control," *Proc. IEEE Int. Symp. Indust. Electron.*, Vol. 1, pp. 543–548, Ajaccio, France, 4–7 May 2004.

13. Karimi, H. R., and Motlagh, M. R. J., "Robust feedback linearization control for a non linearizable MIMO nonlinear system in the presence of model uncertainties," *Proceedings of the IEEE International Conference on Service Operations, Logistics, and Informatics (SOLI '06)*, pp. 965–970, Shanghai, China, 21–23 June 2006.
14. Korayem, M. H., Firouzy, S., and Heidari, A., "Dynamic load carrying capacity of mobile-base flexible-link manipulators: Feedback linearization control approach," *Proceedings of the IEEE International Conference onRobotics and Biomimetics (ROBIO 2007)*, pp. 2172–2177, Sanya, China, 15–18 December 2007.
15. Park, K. C., Chung, H., and Lee, J. G., "Point stabilization of mobile robots via state space exact feedback linearization," *Proc. IEEE Int. Conf. Robot. Automat.*, Vol. 4, pp. 2626–2631, 10–15 May 1999.
16. Sumantri, B., Karsiti, M. N., and Ahmed, S., "Input-output exact feedback linearization for depth positioning of spherical URV," *Proceedings of the International Conference on Advanced Computer Control (ICACC '09)*, pp. 87–91, Singapore, 22–24 January 2009.
17. Buckner, G. D., Schuetze, K. T., and Beno, J. H., "Active vehicle suspension control using intelligent feedback linearization," *Proc. Amer. Control Conf. 2000*, Vol. 6, pp. 4014–4018, 28–30 June 2000.
18. Kwon, J., Kim, T., Jang, J., and Lee, I., "Feedback linearization control of a hydraulic servo system," *Proceedings of the International Joint Conference (SICE-ICASE)*, pp. 455–460, Busan, Korea, 18–21 October 2006.
19. Olivier, P. D., "Feedback linearization of DC motors," *IEEE Trans. Indust. Electron.*, Vol. 38, No. 6, pp. 498–501, December 1991.
20. Lindlau, J. D., and Knospe, C. R., "Feedback linearization of an active magnetic bearing with voltage control," *IEEE Trans. Control Syst. Technol.*, Vol. 10, No. 1, pp. 21–31, January 2002.
21. Lee, D. C., Lee, G., and Lee, K., "DC-bus voltage control of three-phase AC/DC PWM converters using feedback linearization," *IEEE Trans. Industry Appl.*, Vol. 36, No. 3, pp. 826–833, May–June 2000.
22. Miret, J., Vicunia, L. G., Matas, J., Guerrero, J. M., and Cruz, J., "Simplified feedback linearization of a single-phase active power filter using sliding mode control," *Proc. IEEE Int. Symp. Indust. Electron.*, Vol. 2, pp. 869–873, 4–7 May 2004.
23. Savaresi, S. M., "Exact feedback linearization of a fifth-order model of synchronous generators," *IEE Proc. Control Theory Appl.*, Vol. 146, No. 1, pp. 53–57, January 1999.
24. Fregene, K., and Kennedy, D., "Stabilizing control of a high-order generator model by adaptive feedback linearization," *IEEE Trans. Energy Convers.*, Vol. 18, No. 1, pp. 149–156, March 2003.
25. Barret, P., "Method d'etude tres simplifiee des regimes d'oscillations, de petit ou grande amplitude, d'une machine synchrone autur ou a partir d'une position d'equilibres synchrone" [Simplified study of oscillatory states, of small and wide amplitude, of a synchronous machine evolving from a synchronous equilibrium point], in *Electrotechnique Générale, Règimes Transitoires des Machines Tournantes* [*General Electric Theory, Transient Dynamics or Rotating Machines*], France: Universitè de Paris, Sociètè Francaise Des Eletriciens N. 2024, Chap. 7.5, pp. 200–202, 1967.
26. Slotine, J. J., and Lee, W., *Applied Nonlinear Control*, Upper Saddle River, NJ: Prentice-Hall, Chaps. 6 and 7, 1991.
27. Park, J.-W., Harley, R. G., and Venayagamoorthy, G. K., "Adaptive-critic-based optimal neurocontrol for synchronous generators in a power system using MLP/RBF neural networks," *IEEE Trans. Industry Appl.*, Vol. 39, No. 5, pp. 1529–1540, 2003.
28. Bollen, M. H. J., "Voltage sags—characterization," in *Understanding Power Quality Problems: Voltage Sags and Interruptions*, Piscataway, NJ: IEEE Press, Chap. 4, pp. 139–252, 1999.
29. Fornari, F., Procopio, R., and Bollen, M. H. J., "SSC compensation capability of unbalanced voltage sags," *IEEE Trans. Power Delivery*, Vol.20, No. 3, pp. 2030–2037, July 2005.
30. Kirby, B., Kueck, J., Leake, H., and Muhlheim, M., "Nuclear generating stations and transmission grid reliability," *39th North American Power Symposium (NAPS '07)*, pp. 279–287, Las Cruces, NM, 30 September–2 October 2007.

Appendix A

With reference to the assumptions drawn in Section 2, it is possible to define the representation of the synchronous generator in the normal form, recalled in Eq. (1).

Indicating the instantaneous phase value of the network voltage with φ and the Park transformation angle with θ, the following expressions for the network voltage axes components (direct and quadrature) can be obtained:

$$V_d = V\cos(\theta - \varphi), \tag{A1}$$

$$V_q = V\sin(\theta - \varphi), \tag{A2}$$

where V is the RMS per unit value of the network line-to-line voltage. Defining δ as

$$\delta = \varphi - \theta - \frac{\pi}{2}, \tag{A3}$$

it is possible to rewrite Eqs. (A1) and (A2) as

$$V_d = -V\sin\delta, \tag{A4}$$

$$V_q = -V\cos\delta. \tag{A5}$$

The expressions linking the generator voltage to the network voltage in per-unit and in the Park domain can be obtained as follows:

$$V_{md} = -\omega_e X i_q - V\sin\delta, \tag{A6}$$

$$V_{mq} = \omega_e X i_d - V\cos\delta, \tag{A7}$$

where $V_{md(q)}$ is the direct (quadrature) axis machine voltage, $i_{d(q)}$ are the current axes components, and X is the inductive reactance modeling the line and the step-up transformer connecting the machine to the main grid.

Now consider, respectively, the machine electric and magnetic equations. As far as the first ones are concerned, the following relations hold:

$$V_{md} = \omega_e \Phi_q, \tag{A8}$$

$$V_{mq} = -\omega_e \Phi_d, \tag{A9}$$

$$V_f = R_f i_f + \frac{1}{\omega_n}\dot{\Phi}_f, \tag{A10}$$

with Φ_d and Φ_q being the axes components of the stator fluxes, V_f the field voltage, R_f the field resistance, i_f the field current, and Φ_f the field flux.

With regard to the magnetic equations, they can be written in terms of expressions linking current and fluxes:

$$\Phi_d = X_d i_d + X_{md} i_f, \tag{A11}$$

$$\Phi_q = X_q i_q, \tag{A12}$$

$$\Phi_f = X_f i_f + X_{md} i_d, \tag{A13}$$

where X_d and X_q are the machine axes reactances, X_{md} is the magnetizing direct axis reactance, and X_f is the field reactance. Referring to [2], the following form of the electromagnetic torque can be derived:

$$T_e = \Phi_q i_d - \Phi_d i_q + K_d(\omega_e - \omega), \tag{A14}$$

where ω is the machine speed, and the coefficient K_d is a damping factor [25], representing the effect of the dampers (neglected in the present model) in a simplified way by adding an equivalent asynchronous torque, defined as

$$K_d = \frac{3V_R^2 \tau_d''}{\omega_e(X + X_d'')}, \tag{A15}$$

where τ_d'' and X_d'' are, respectively, the direct axis short-circuit sub-transient time constant and sub-transient reactance, and V_R is the machine rated voltage.

Then consider the mechanical equation, starting from the well-known motion law

$$T_e - T_m = 2H\dot{\omega}, \tag{A16}$$

with being H the inertia constant and the dynamic equation of the angle δ

$$\dot{\delta} = \omega_n(\omega - \omega_e). \tag{A17}$$

Considering Eqs. (A10), (A16), and (A17), it is possible to define a system state vector $\boldsymbol{x}$ of dimension (3×1) as

$$\boldsymbol{x} = [x_1 \quad x_2 \quad x_3]^T = [\delta \quad \omega \quad \Phi_f]^T. \tag{A18}$$

Now, system inputs are chosen for the field voltage V_f and the prime mover mechanical torque T_m, namely

$$\boldsymbol{u} = [u_1 \quad u_2]^T = [V_f \quad T_m]^T. \tag{A19}$$

Defining the transient reactance X_d' as

$$X_d' = X_d - \frac{X_{md}^2}{X_f} \tag{A20}$$

after some algebraic manipulations of the two blocks of Eqs. (A6)–(A14) and (A16) and (A17), the following expressions for $\boldsymbol{f}(\boldsymbol{x})$ and $\boldsymbol{g}(\boldsymbol{x})$ vectors can be obtained:

$$\boldsymbol{f}(\boldsymbol{x}) = \begin{bmatrix} \omega_n(\omega - \omega_e) \\ AB\sin 2\delta - AC\Phi_f \sin\delta + \dfrac{K_d}{2H}(\omega_e - \omega) \\ D\Phi_f + E\cos\delta \end{bmatrix}, \tag{A21}$$

$$\boldsymbol{g}(\boldsymbol{x}) = \begin{bmatrix} 0 & 0 \\ 0 & -\dfrac{1}{2H} \\ \omega_n & 0 \end{bmatrix}, \tag{A22}$$

where A, B, C, D, and E are suitable constants, depending on the system parameters, defined as

$$\begin{cases} A = -\dfrac{V}{2H(X + X_q)(X + X'_d)\omega_e} \\ B = \dfrac{V}{2\omega_e}(X_q - X'_d) \\ C = \dfrac{(X + X_q)X_{md}}{X_f} \\ D = \dfrac{R_f \omega_n \left[X X_{md}^2 - X_f X_d (X + X'_d)\right]}{X_f^2 X'_d (X + X'_d)} \\ E = \dfrac{R_f \omega_n X_{md} V}{X_f \omega_e (X + X'_d)} \end{cases}. \tag{A23}$$

To complete the system formulation, one has now to derive the system outputs equations in relation to the states. Start with the definition of the machine voltage

$$V_m^2 = V_{md}^2 + V_{mq}^2. \tag{A24}$$

It is possible to rewrite Eq. (A24) using Eqs. (A6)–(A13), giving

$$V_m^2 = A_h \sin^2 \delta + B_h \cos^2 \delta + C_h \Phi_f^2 + D_h \Phi_f \cos \delta, \tag{A25}$$

where the constants A_h, B_h, C_h, and D_h are defined as

$$\begin{cases} A_h = \dfrac{V^2 X_q^2}{(X + X_q)^2} \\ B_h = \dfrac{V^2 X_d'^2}{(X + X'_d)^2} \\ C_h = \dfrac{\omega_e^2 X^2 X_{md}^2}{X_f^2 (X'_d + X)^2} \\ D_h = 2\dfrac{\omega_e X X_{md} X'_d V}{X_f (X'_d + X)^2} \end{cases}. \tag{A26}$$

The electromagnetic power can be derived easily from the electromagnetic torque equation as

$$P_e = T_e \omega_e. \tag{A27}$$

Using the results from Eqs. (A6)–(A14), P_e becomes

$$P_e = E_h \sin 2\delta + F_h \Phi_f sin\delta + K_d \omega_e (\omega_e - \omega), \tag{A28}$$

with

$$\begin{cases} E_h = \dfrac{V^2(X'_d - X_q)}{2\omega_e(X + X_q)(X + X'_d)} \\ F_h = \dfrac{VX_{md}}{X_f(X + X'_d)} \end{cases} . \tag{A29}$$

This way, with reference to Eq. (1), the expression of the vector $\boldsymbol{h}(\boldsymbol{x}) = [h_1(x)\ \ h_2(x)]^T$ can finally be written, which is necessary to complete the system formulation in its normal form:

$$\begin{cases} h_1(\boldsymbol{x}) = E_h \sin 2\delta + F_h \Phi_f \sin\delta + K_d \omega_e(\omega_e - \omega) \\ h_2(\boldsymbol{x}) = A_h \sin^2\delta + B_h \cos^2\delta + C_h \Phi_f^2 + D_h \Phi_f \cos\delta \end{cases} . \tag{A30}$$